Variable-kinematic finite beam elements and viscous-spring artificial boundary for wave propagation in infinite space

Journal of Mechanics, 2025, **41**, 129–136
https://doi.org/10.1093/jom/ufaf010
Regular Article

OXFORD

Variable-kinematic finite beam elements and viscous-spring artificial boundary for wave propagation in infinite space

Xinzhu Li [1,*], Yunqiu Song [1], Rodolfo Azzara [2], Matteo Filippi [2] and Erasmo Carrera [2,3]

[1]The First Aircraft Institute, AVIC, Renmindong Street 1, 710089 Xi'an, People's Republic of China
[2]Department of Mechanical and Aerospace Engineering, Politecnico di Torino, Corso Duca degli Abruzzi 24, 10129 Torino, Italy
[3]Department of Mechanical Engineering, College of Engineering, Prince Mohammad Bin Fahd University, Al-Khobar, Kingdom of Saudi Arabia

*Corresponding author: lixinzhu5211@163.com

ABSTRACT

This paper uses the viscous-spring artificial boundary method and variable-kinematic finite beam elements to solve wave propagation problems in infinite space. According to the artificial boundary technique, springs and dashpots with appropriate elastic and damping coefficients are applied at the external surfaces of the domain to ensure the absorption of the incident waves. The finite-element matrices and vectors corresponding to various 1-dimensional kinematic models are obtained with the Carrera Unified Formulation. In particular, using Lagrange-type expansions for approximating the primary variables over the finite beam element cross-section has enabled the artificial boundaries to be easily applied. Both outer- and inner-source problems have been considered to compare the methodology with analytical and numerical solutions available in the literature. Moreover, the current approach has been adopted to solve wave propagation problems of a configuration consisting of a semi-infinite space and a beam-like structure on its free surface and subjected to various loading conditions.

KEYWORDS: Carrera Unified Formulation, beam model, wave propagation, viscous-spring boundary method

1 INTRODUCTION

Wave propagation prediction in infinite media is crucial in many research fields, such as acoustics, seismology and aircraft engineering. Numerical methods were essential for the researching and engineering fields because analytical solutions were commonly available for specific conditions, such as limitations of media or boundary conditions [1–4]. Furthermore, in aircraft engineering, the finite-element (FE) method was commonly used to perform strength verification on structural components of aircraft under various operating conditions, for example, simulating the far field scattering problem of aircraft far from the incident wave source. The FE method [5] enables complex domains and material properties to be easily handled. For instance, the FE approach was employed to model composite meta-structures conceived for vibration absorption [6] and evaluate the effect of thermal relaxation time in poroelastic materials [7].

Meanwhile, simulating wave propagation in infinite space or with truncated boundaries due to excessively large computational models by using a numerical method requires the application of appropriate boundary conditions [8,9] to reduce the computational domain to be discretized. These conditions can be classified into two main categories: (1) global and (2) local artificial boundaries. The global approach ensures that the outgoing wave across the outer surfaces satisfies all the field equations and physical boundary conditions in the infinite domain. Some methodologies presented in the literature that fall into this category are the boundary element method [10], series solutions, and the infinite-element method [11]. On the other hand, the local artificial methodology guarantees that the outgoing wave at any point of the artificial boundary passes through the border itself [12]. The Sommerfield boundary [13], viscous boundary [14], transmission boundary [15] and viscous-spring artificial boundary (VSAB) [16] are some strategies based on this concept. In particular, the VSAB uses simple mechanical analogs consisting of springs, dashpots and (sometimes) mass elements to simulate the far-field infinite space surrounding the FE domain [17]. Thanks to its simplicity and flexibility, the VSAB approach has been utilized for exploring wave propagation transient mechanisms within 3-dimensional (3D) [18], cylindrical [19] and porous [20] media.

This work combines high-fidelity finite beam elements developed with the Carrera Unified Formulation (1D-CUF) and the VSAB strategy to investigate wave propagation problem in isotropic infinite spaces. CUF is a hierarchical formulation that automatically enables one to conceive FE formulations based on arbitrary kinematic (or structural) theories. For pure elastic problems, the primary variables, namely the 3 components of the displacement field, are approximated by using products by arbitrary functions of the cross-section coordinates and the FE shape functions defined along the beam axis. The number and the nature of the cross-sectional functions are input parameters of the analysis. The accuracy and computational efficiency of the CUF elements have been demonstrated in various engineering applications, including static [21,22], dynamic [23–26],

Received: 5 November 2024; **Revised:** 6 February 2025; **Accepted:** 14 March 2025

stability [27,28], multi-field [29] and multi-scale [30,31] analyses. At present, CUF is commonly used for studying the mechanical analysis of structures, which have finite geometric boundaries. This paper innovatively attempts to establish VSAB based on CUF, which can be used to study the propagation of elastic waves in infinite or semi-infinite regions, expanding the application scenarios of the CUF method. In addition, it is known from existing literature that VSAB is often implemented through commercial finite-element software, and the combination of VSAB and CUF in this paper is novel and constructive, which balances the stability and effectiveness of VSAB with the high efficiency and accuracy of CUF, providing a foundation for future research on a wider range of applications.

This paper is organized as follows: (i) the CUF and VSAB formulations are presented in Section 2; (ii) Section 3 presents some numerical results, showing the validity and accuracy of the proposed methodology; and, finally, (iii) the conclusions are given in Section 4.

2 ARTIFICIAL BOUNDARY CONDITION IN CUF FORM

We consider a Cartesian reference system (x, y, z), whose x–z plane and the y-direction define the cross-section and the longitudinal axis of a 3D beam structure, respectively. The body is elastic, and the deformations are assumed to be small, so the geometrical and constitutive relations remain linear.

$$\begin{aligned} \epsilon &= Du, \\ \sigma &= C\epsilon. \end{aligned} \tag{1}$$

The matrices D and C, respectively, represent the linear differential operator and the tensor of material coefficients that relate the displacement $u(x, y, z)$, strain $\epsilon(x, y, z)$ and stress $\sigma(x, y, z)$ vectors. According to the 1D formalism of the unified formulation, the displacement field is written as follows:

$$\mathbf{u}(x, y, z; t) = F_\tau(x, z)\,\mathbf{u}_\tau(y; t), \qquad \tau = 1, 2, \ldots, M, \tag{2}$$

where $\mathbf{u}_\tau$ is the vector of the generalized displacements, F_τ is cross-sectional functions and determine the class of the 1D-CUF model and M is the number of terms included in the kinematic expansion. The generalized displacements can be approximated over the beam axis by using the conventional FE shape functions, $N_i(y)$. Thus, Eq. (2) becomes

$$\mathbf{u}(x, y, z; t) = F_\tau(x, z) N_i(y)\,\mathbf{q}_{\tau i}(t), \qquad i = 1, 2, \ldots, n_{el}, \tag{3}$$

in which $\mathbf{q}_{\tau i}(t)$ is the vector of the nodal unknowns, n_{el} denotes the number of nodes per element, and the subscripts τ and i indicate summation.

The equations of motion are formulated using the principle of virtual work that establishes the well-known equilibrium relation between the virtual strain energy δL_{int}, and the virtual works done by inertial δL_{iner}, viscous δL_{damp} and external δL_{ext} forces.

$$\delta L_{int} + \delta L_{iner} + \delta L_{damp} = \delta L_{ext}. \tag{4}$$

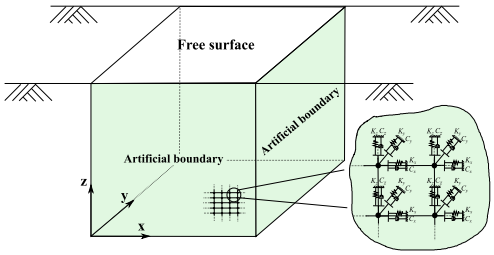

Figure 1 Model for the viscous-spring artificial boundary, where the artificial boundaries are represented by colored areas.

The substitution of Eqs. (3) and (1) into Eq. (4) leads to the following expressions:

$$\begin{aligned} \delta L_{int} &= \delta \mathbf{q}_{\tau i}^T \mathbf{K}_s^{ij\tau s} \mathbf{q}_{sj}, \\ \delta L_{ine} &= \delta \mathbf{q}_{\tau i}^T \mathbf{M}^{ij\tau s} \ddot{\mathbf{q}}_{sj}, \\ \delta L_{damp} &= \delta \mathbf{q}_{\tau i}^T \mathbf{C}^{ij\tau s} \dot{\mathbf{q}}_{sj}, \\ \delta L_{ext} &= \delta \mathbf{q}_{\tau i}^T \mathbf{F}^{\tau i}, \end{aligned} \tag{5}$$

where $\mathbf{K}_s^{ij\tau s}$, $\mathbf{M}^{ij\tau s}$, $\mathbf{C}^{ij\tau s}$and $\mathbf{F}^{\tau \mathrm{i}}$ represent the so-called *fundamental nuclei* of the stiffness matrix, mass matrix, damping matrix and external load vector, respectively. The overdot stands for time differentiation. The additional indexes s and j are used to express the virtual displacement vector in the unified formulation $\delta\mathbf{u}(x, y, z; t) = F_s(x, z) N_j(y)\,\mathbf{q}_{sj}(t)$ and they have the bounds of τ and i, respectively. The global FE matrices and vectors related to arbitrary kinematic expansions are automatically obtained by permuting the 4 indexes and assembling the *fundamental nuclei* [32]. Eventually, the equations of motion in the time domain are as follows:

$$\mathbf{M}\ddot{\mathbf{q}}(t) + \mathbf{C}\dot{\mathbf{q}}(t) + \mathbf{K}_s\mathbf{q} = \mathbf{F}(t). \tag{6}$$

The Newmark time integration scheme is employed to solve the system. For the sake of brevity, readers are referred to [23,33] for details about this integration scheme.

As the choice of F_τ and M is arbitrary, the basis functions available to simulate the displacement field at the cross-section can be varied and extended to any order [34]. We have adopted 2D Lagrange-type polynomials (LE) to derive the structural theory in this work [35–38]. According to the LE approach, the structure's cross-section is discretized using an arbitrary number of 2D sub-domains (or sectional elements) delimited by some points (or sectional nodes). Over each element, the kinematic field is expressed as a linear combination of Lagrange-type polynomials whose order is determined by the number of sectional nodes. Thus, bi-linear, bi-quadratic and bi-cubic Lagrange polynomials can be obtained using quadrilateral elements with 4, 9 and 16 points. The LE approach has two main features: (1) the kinematic field approximation can be varied locally and (2) the primary unknowns are the displacements of the sectional nodes. In particular, the second feature is shared with the conventional solid FE formulations and significantly facilitates the application of the local artificial boundaries. Figure 1 schematically shows a generic 3D domain discretized with bi-linear elements. A mechanical analog is applied at each node belonging to the

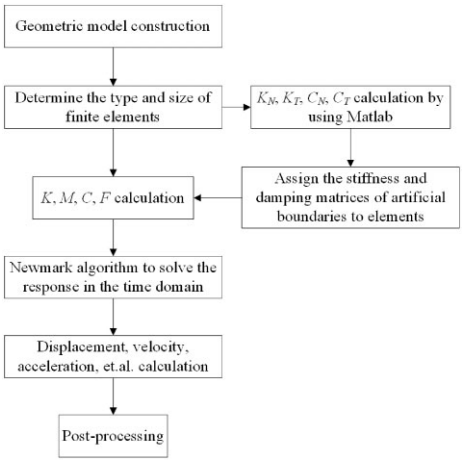

Figure 2 Implementation of viscoelastic artificial boundary flowchart based on the CUF framework FE model.

5 truncated surfaces to ensure the transmitting conditions of an infinite media.

The K_i and C_i values represent the elastic and damping coefficients along the three directions $i = x, y, z$ of the springs and dashpots of the mechanical analogs and they are defined as follows:

$$K_N = A_l \cdot \frac{1}{1+A}\frac{\lambda+G}{r}, \qquad C_N = A_l \cdot B\rho c_p,$$
$$K_T = A_l \cdot \frac{1}{1+A}\frac{G}{r}, \qquad C_T = A_l \cdot B\rho c_s, \tag{7}$$

where N and T denote the perpendicular and tangent directions of the plane where the boundary nodes are located, A_l is the total truncated boundary area of all elements containing the boundary node l, and A and B are the modified coefficients with the value of 0.8 and 1.1 [39], which are obtained from a number of tests for good wave absorption. λ and G stand for the Lamé constants, r indicates the distance between the wave source and the nodes on the artificial boundary, C_s and C_p are the shear wave velocity and compression wave velocity, respectively, and ρ is the density.

Based on the derivation of the above functions, Fig. 2 shows the process of implementing viscoelastic artificial boundaries using the FE model under the CUF framework.

3 NUMERICAL EXAMPLES

The outlined approach for simulating various boundary conditions has been assessed in this section. First, the deflections of a beam-like structure were calculated by varying the stiffness coefficients of springs applied to its ends. Then, we analyzed waves' propagation due to outer- and inner sources within infinite and semi-infinite homogeneous media.

3.1 Static analyses of a beam-like structure

The beam-like structure and the boundary conditions are shown in Fig. 3. The structure was made of an isotropic material with Young's modulus $E = 75$ GPa, Poisson's ratio $\nu = 0.33$ and density $\rho = 2700$ kg/m^3. The mathematical model consisted of ten 4-node finite beam elements along the y-axis and a bi-

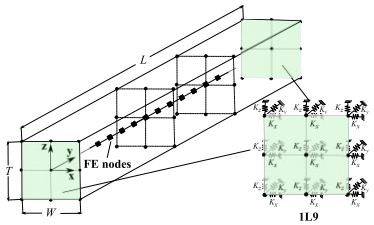

Figure 3 The beam-like configuration with $L = 20, W = T = 0.2$ m.

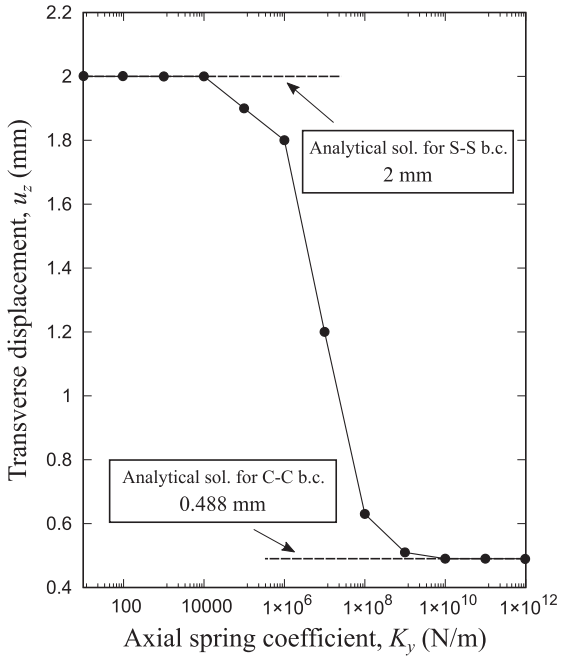

Figure 4 Transverse deflection versus axial spring coefficient ($K_x = K_y$ and $K_z = 10^{12}$ N/m).

quadratic (L9) Lagrange element over the cross-section. Springs have been applied at the nodes of the cross-section at $y = 0$ and 20 m, and their coefficients have been varied to simulate both elastic and rigid supports.

Figure 4 shows the maximum deflections in the z-direction due to a concentrated load $F = 1$ kN applied at the beam mid-span. For comparison purposes, we reported the analytical results for simply supported (S-S) and clamped–clamped (C-C) boundary conditions (b.c.) calculated with the following formulas: $u_z = \frac{FL^3}{48EI}$ and $u_z = \frac{FL^3}{192EI}$, where I is the moment of inertia. Both configurations were accurately simulated by varying the stiffness values of the axial spring K_y.

3.2 The Lamb problem

The first wave propagation analysis was carried out considering the domain shown in Fig. 5. The material properties were the following: density $\rho = 1800$ kg/m^3, shear wave velocity $C_s = 500$ m/s and Poisson's ratio $\nu = 0.25$. The viscous-spring boundary conditions were applied to the bottom and lateral surfaces, while a concentrated force was exerted on the top free surface.

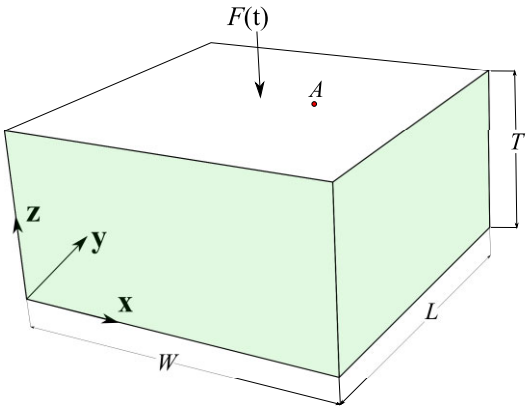

Figure 5 Computational domain and load condition for the Lamb problem with the dimensions $L = 100$, $W = 100$, and $T = 50$ m.

The load varied in time according to the following equation:

$$F(t) = 16F_0\left[\left(\frac{t}{T_0}\right)^3 H\left(\frac{t}{T_0}\right) - 4\left(\frac{t}{T_0} - \frac{1}{4}\right)^3 H\left(\frac{t}{T_0} - \frac{1}{4}\right) + 6\left(\frac{t}{T_0} - \frac{1}{2}\right)^3 H\left(\frac{t}{T_0} - \frac{1}{2}\right) - 4\left(\frac{t}{T_0} - \frac{3}{4}\right)^3 \times H\left(\frac{t}{T_0} - \frac{3}{4}\right) + \left(\frac{t}{T_0} - 1\right)^3 H\left(\frac{t}{T_0} - 1\right)\right], \quad (8)$$

where $H(*)$ represents the Heaviside function, $F_0 = 10$ GN is the peak value of impulse and $T_0 = 1.0$ s denotes the acting time of impulse. Figure 6-(a) shows the transverse displacements at the point $A(70, 50, 50)$ belonging to the free boundary calculated with various 1D-CUF models.

The comparisons with the analytical solution revealed that the discretization consisting of 10 bi-quadratic (10L9) elements over the cross-section and five 3-node beam elements (5B3) led to a convergent solution with the minimum number of degrees of freedom (DOF). Taking the black curve 50L4&10B2-726DOF in Fig. 6(a) as an example, 50L4 means fifty 4-node linear elements and 10B2 means ten 2-node beam elements, with a total of 726 degrees of freedom. On the other hand, the linear formulations, namely models with L4 and B2 elements, required a higher computational effort to predict the correct peak value. Moreover, we evaluated the effects on the response of the time-step used in the integration scheme by employing the 10L9&5B3 model [see Fig. 6(b)]. The results demonstrated that a Δt equal to 0.01 s provided a convergent solution. However, regardless of which spatial and temporal discretizations have been considered, there are slight discrepancies with respect to the analytical result at 0.4–0.5 s. These mismatches have already been observed in [18] and can be ascribed to the intrinsic numerical deficiencies of VSAB and FE procedures. In the simulation calculation using a personal laptop equipped with an R5-4600U CPU and 16 GB RAM, the 10L9&5B3 case with minimal DOF required 184 s to achieve convergence. The computational errors between simulation results and analytical solutions at different time-steps are shown in Table 1.

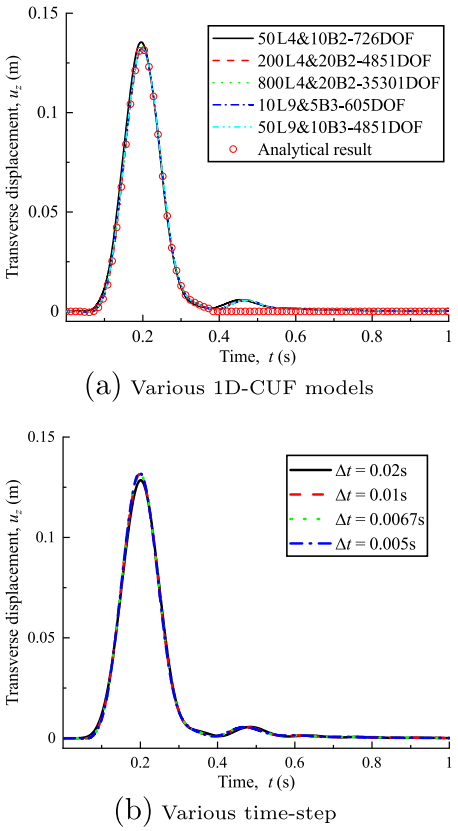

Figure 6 Transverse displacement at the point A(70,50,50) for the Lamb problem: (a) different mesh approximations and (b) time-step used in the integration scheme.

Table 1. Computational errors between simulation results and analytical solutions.

Time/s	0.1	0.15	0.2	0.25	0.3	0.35
Error	11.46%	2.66%	0.03%	0.35%	2.72%	2.86%

Finally, Fig. 7 shows the propagation wave on the free surface at various instants. The simulation was performed by assuming a lower value of the shear wave velocity than the previous example, namely $C_s = 75$ m/s. It should be observed that the wave was properly absorbed at 0.942 s by the artificial boundaries.

3.3 The inner-source problem

Contrary to the previous case, the VSAB conditions have been applied to all six boundary surfaces for the inner-source problem (see Fig. 8). The CUF-FE model consisted of 25 bi-quadratic Lagrange elements over the cross-section and five 3-node beams along the y-axis. On the other hand, the force and material data were the same as in the previous case.

Figure 9(a) and (b) shows the transverse displacements of points $A(55,55,55)$ and $B(70,50,50)$ as functions of time. Although the current numerical method is based on 1D FE discretization, it perfectly reproduced the solutions deriving from

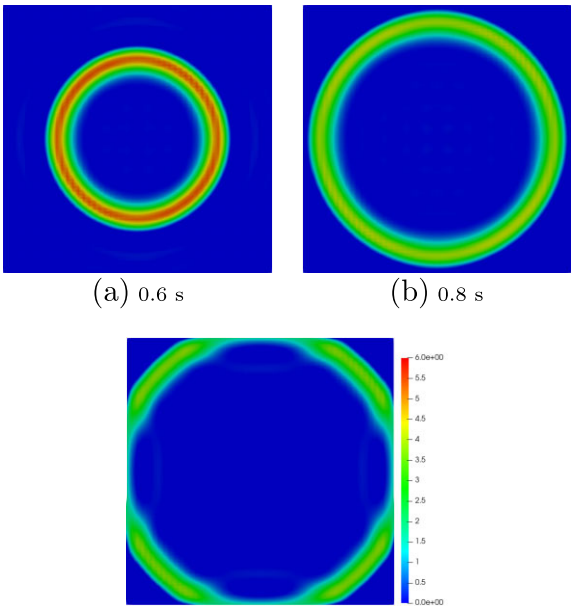

Figure 7 Propagating wave over the free surface.

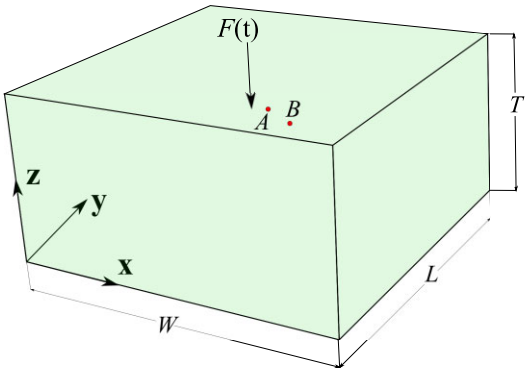

Figure 8 Computational domain and load condition for the inner-source problem with the dimensions $L = 100$, $W = 100$ and $T = 100$ m.

the solid FE model and the analytical formulation proposed in [18].

Furthermore, contrary to what happened for the Lamb problem, we did not observe any discrepancies between the FE models and the analytical solution.

3.4 Superstructure under various loading conditions

The following numerical simulations concerned the responses of a domain consisting of the semi-infinite space considered in the Lamb problem and an additional structure placed above its free surface. This configuration was subjected to 3 different point forces, as shown in Fig. 10, which were applied independently. Equation (8) reports their time histories by assuming $F_0 = 50$ kN and $T_0 = 0.5$.

The domain was made of an isotropic material whose properties were as follows: density $\rho = 1800$ kg/m^3, shear wave velocity $C_s = 50$ m/s and Poisson's ratio $\nu = 0.25$. The 1D-CUF

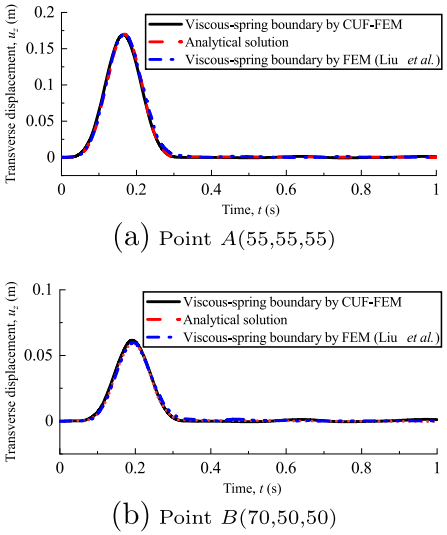

Figure 9 Transverse displacements at 2 reference points for the inner-source problem and comparison with the analytical solution and the 3D-FE results of [18].

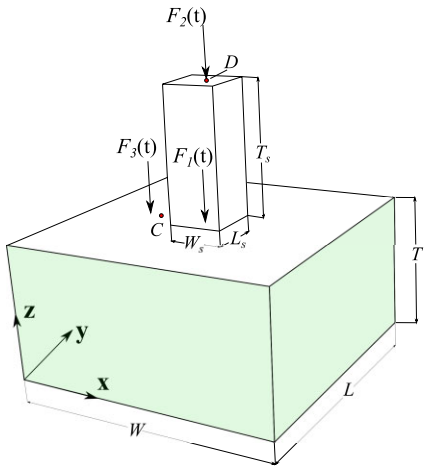

Figure 10 Computational domain and various load conditions for the superstructure problem with the dimensions $L = 100$, $W = 100$, $T = 50$, $L_s = 20$, $W_s = 20$ and $T_s = 50$ m.

model consisted of 50L9&10B3 for the semi-infinite space and 10L9&2B3 for the remaining part.

In Fig. 10, the observation points C and D are located on the surface of the half-space and the top of the superstructure, respectively. Three loading cases are set up, and the coordinates of the force application points are (50,50,50), (50,50,100) and (30,50,50). It can be seen that the 3 loading cases have no obvious effect on the maximum displacement amplitude of observation point C, but have a significant effect on observation point D. The displacement generated by force F_2 at the observation point D is significantly higher than that in the other two cases, because when force F_1 or F_3 acts, most of the energy of the stress wave propagates in semi-infinite space, that is, absorbed by the artificial boundary, and only a small part propagates to observation point D.

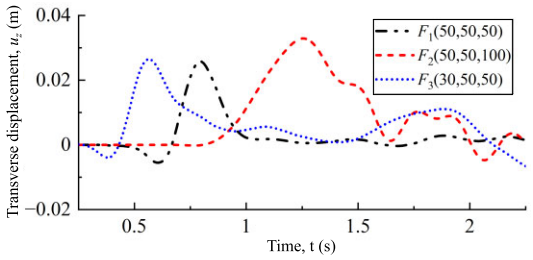

(a) Point $C(35,50,50)$

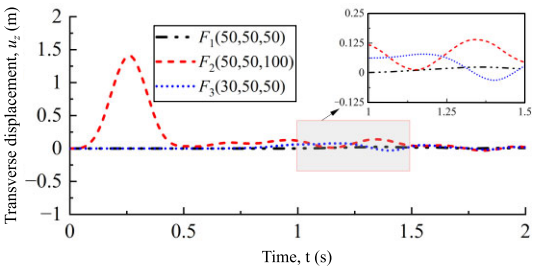

(b) Point $D(50,50,100)$

Figure 11 Transverse displacements calculated at the observation points of Fig. 10.

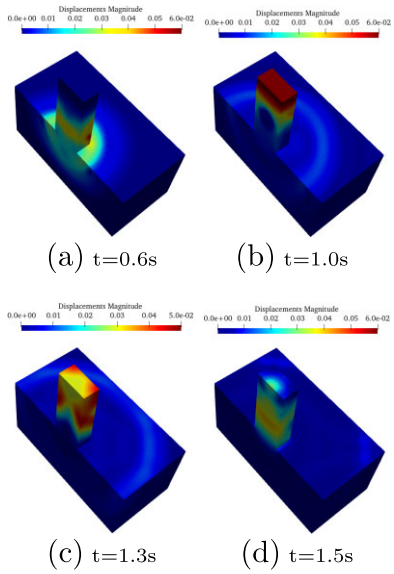

Figure 12 Displacement magnitude on the section at $y = 50$ under the force $F_1(50, 50, 50)$.

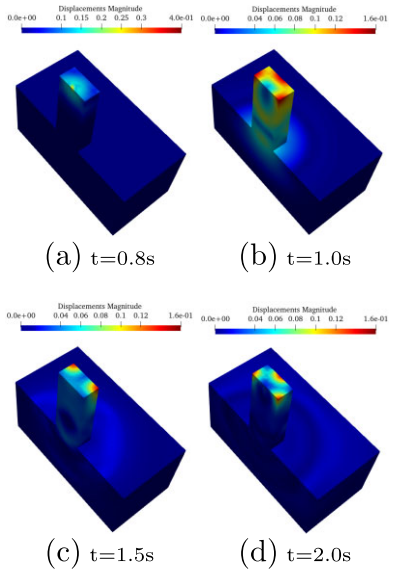

Figure 13 Displacement magnitude on the section at $y = 50$ under the force $F_2(50, 50, 100)$.

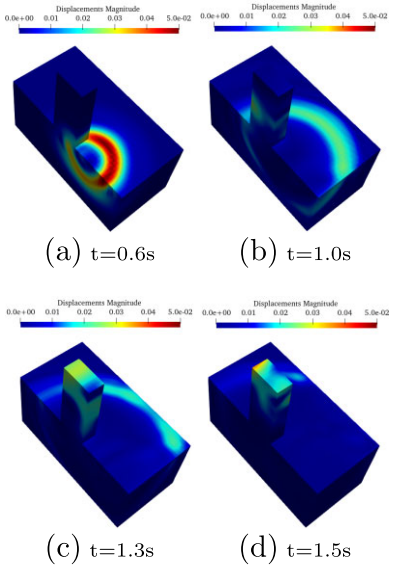

Figure 14 Displacement magnitude on the section at $y = 50$ under the force $F_3(30, 50, 50)$.

Figure 11 shows the transverse displacements of 2 points for the 3 loading conditions. Figures 12–14 show how the wave propagated for the 3 cases. As previously mentioned, the most significant deformations were obtained when the force acted on the top of the superstructure. Moreover, it can be observed that the artificial boundaries absorbed the waves in all cases, simulating the transmitting condition correctly.

4 CONCLUSION

This paper combined the VSAB technique with variable-kinematic finite beam elements derived with a CUF , and the obtained absorbing boundary could effectively solve the simulation problems of unbounded wave propagation. This paper adopted the Lagrange-type kinematics to approximate the primary variables over the plane orthogonal to the finite beam elements' axis. The accuracy of the CUF-VSAB methodology was demonstrated by considering simple static and wave problems for which analytical and high-fidelity numerical solutions are available. Although the proposed approach was based on 1D formulations, it provided results comparable to those obtained with the 3D FE solutions. In addition, the flexibility of the present method allowed the modeling of a more complex configuration consisting of a semi-infinite space and a beam-like structure. Three different loading conditions were considered to evaluate the effect of

the force location on the superstructure's deformations and the absorption capabilities of the artificial boundaries.

ACKNOWLEDGMENTS

The authors thank the anonymous reviewers for their valuable suggestions.

AUTHOR CONTRIBUTIONS

X.L. and Y.S. conducted the theoretical derivation and verification, R.A. and X.L. analyzed the results, X.L. and R.A. wrote and reviewed the manuscript, and E.C. and M.F. provided theoretical support.

CONFLICT OF INTEREST STATEMENT

None declared.

REFERENCES

1. Achenbach J. *Wave Propagation in Elastic Solids*. Amsterdam, Netherlands: North-Holland, 2012.
2. Sezawa K. *Scattering of elastic waves and some allied problems*. Bulletin of the Earthquake Research Institute, Tokyo Imperial University 1927;**3**:19–41.
3. Song YQ, Li XZ, Yang Y, Sun MH, Yang ZL, Fang XQ. Scattering of anti-plane (SH) waves by a hill with complex slopes. *Journal of Earthquake Engineering* 2020;**2**:1–21.
4. Seriani G, Oliveira SP. Numerical modeling of mechanical wave propagation. *La Rivista del Nuovo Cimento*, 2020;**43**(9):459–514.
5. Liu WK, Li S, Park H. Eighty years of the finite element method: birth, evolution, and future. *Archives of Computational Methods in Engineering* 2022;**29**:4431–4453.
6. Matlack KH, Bauhofer A, Krödel S, Palermo A, Daraio C. Composite 3D-printed metastructures for low-frequency and broadband vibration absorption. *Proceedings of the National Academy of Sciences*, 2016;**113**(30):8386–8390.
7. Saeed T, Abbas I, Marin M. A GL model on thermo-elastic interaction in a poroelastic material using finite element method. *Symmetry*, 2020;**12**(3):488.
8. Engquist B, Majda A. Absorbing boundary conditions for numerical simulation of waves. *Proceedings of the National Academy of Sciences*, 1977;**74**(5):1765–1766.
9. Clayton R, Engquist B. Absorbing boundary conditions for acoustic and elastic wave equations. *Bulletin of the Seismological Society of America*, 1977;**67**(6):1529–1540.
10. Stamos AA, Beskos DE. Dynamic analysis of large 3D underground structures by the bem. *Earthquake Engineering & Structural Dynamics*, 1995;**24**(6):917–934.
11. Zhu W, Ding C, Zhao X. A numerical method for designing acoustic cloak with homogeneous metamaterials. *Applied Physics Letters*, 2010;**97**(13):131902.
12. Givoli D. High-order local non-reflecting boundary conditions: a review. *Wave Motion*, 2004;**39**(4):319–326.
13. Sommerfeld A. *Partial Differential Equations in Physics*. New York, USA: Academic Press, 1949.
14. Lysmer J, Kuhlemeyer RL. Finite dynamic model for infinite media. *Journal of the Engineering Mechanics Division*, 1969;**95**(4):859–877.
15. Liao ZF, Huang KL, Yang BP, Yuan YF. A transmitting boundary for transient wave analyses. *Science in China Series A—Mathematics, Physics, Astronomy & Technological Science*, 1984;**27**(10):1063–1076.
16. Liu JB, Lu YD. A direct method for analysis of dynamic soil–structure interaction based on interface idea. *Developments in Geotechnical Engineering*, 1998;**83**:261–276.
17. Deeks AJ, Randolph MF. Axisymmetric time-domain transmitting boundaries. *Journal of Engineering Mechanics*, 1994;**120**(1):25–42.
18. Liu J, Du Y, Du X, Wang Z, Wu J. 3D viscous-spring artificial boundary in time domain. *Earthquake Engineering and Engineering Vibration*, 2006;**5**(1):93–102.
19. Du X, Zhao M. A local time-domain transmitting boundary for simulating cylindrical elastic wave propagation in infinite media. *Soil Dynamics and Earthquake Engineering*, 2010;**30**(10):937–946.
20. Xu C, Song J, Du X, Zhao M. A local artificial-boundary condition for simulating transient wave radiation in fluid-saturated porous media of infinite domains. *International Journal for Numerical Methods in Engineering*, 2017;**112**(6):529–552.
21. Pagani A, Azzara R, Augello R, Carrera E, Wu B. Accurate through-the-thickness stress distributions in thin-walled metallic structures subjected to large displacements and large rotations. *Vietnam Journal of Mechanics*, 2020;**42**(3):239–254.
22. Carrera E, Petrolo M. Refined beam elements with only displacement variables and plate/shell capabilities. *Meccanica*, 2012;**47**(3):537–556.
23. Azzara R, Carrera E, Filippi M, Pagani A. Time response stress analysis of solid and reinforced thin-walled structures by component-wise models. *International Journal of Structural Stability and Dynamics*, 2020;**20**(14):2043010.
24. Azzara R, Filippi M, Pagani A. Variable-kinematic finite beam elements for geometrically nonlinear dynamic analyses. *Mechanics of Advanced Materials and Structures*, 2023;**30**(20):4146–4154.
25. Filippi M, Carrera E, Regalli AM. Layerwise analyses of compact and thin-walled beams made of viscoelastic materials. *Journal of Vibration and Acoustics* 2016;**138**(6):064501.
26. Li XZ, Song YQ, Filippi M, Azzara R, Yang ZL, Carrera E. Evaluation of the effects of the seismic wave incidence angle on soil-structure interactions via advanced finite beam elements. *Mechanics of Advanced Materials and Structures*, 2024;**31**(1):103–116.
27. Carrera E, Azzara R, Daneshkhah E, Pagani A, Wu B. Buckling and post-buckling of anisotropic flat panels subjected to axial and shear in-plane loadings accounting for classical and refined structural and nonlinear theories. *International Journal of Non-Linear Mechanics* 2021;**133**:103716.
28. Pagani A, Azzara R, Augello R, Carrera E. Stress states in highly flexible thin-walled composite structures by unified shell model. *AIAA Journal*, 2021;**59**(10):4243–4256.
29. Entezari A, Filippi M, Carrera E, Kouchakzadeh MA. 3D-wave propagation in generalized thermoelastic functionally graded disks. *Composite Structures* 2018;**206**:941–951.
30. Kaleel I, Petrolo M, Waas AM, Carrera E. Computationally efficient, high-fidelity micromechanics framework using refined 1D models. *Composite Structures* 2017;**181**:358–367.
31. Carrera E, de Miguel AG, Filippi M, Kaleel I, Pagani A, Petrolo M, Zappino E. Global-local plug-in for high-fidelity composite stress analysis in ABAQUS. *Mechanics of Advanced Materials and Structures*, 2021;**28**(14):1445–1450.
32. Carrera E, Cinefra M, Petrolo M, Zappino E. *Finite Element Analysis of Structures through Unified Formulation*. Chichester: John Wiley & Sons, 2014.
33. Newmark NM. A method of computation for structural dynamics. *Journal of the Engineering Mechanics Division*, 1959;**85**(3):67–94.
34. Carrera E, Giunta G, Petrolo M. *Beam Structures: Classical and Advanced Theories*. West Sussex, UK: John Wiley & Sons, 2011.
35. Carrera E. Multilayered shell theories accounting for layerwise mixed description. I—governing equations. *AIAA Journal* 1999;**37**:1107–1116.
36. Pagani A, Carrera E, Augello R, Scano D. Use of Lagrange polynomials to build refined theories for laminated beams, plates and shells. *Composite structures* 2021;**276**:114505.

37. Carrera E, Pagani A, Petrolo M, Zappino E. A component-wise approach in structural analysis. In: Topping BHV (ed). *Computer Methods for Engineering Sciences*. Stirlingshire, UK: Saxe–Coburg Publications, Chapter 4, 2012, 75–115.
38. Pagani A, Carrera E. Unified formulation of geometrically nonlinear refined beam theories. *Mechanics of Advanced Materials and Structures*, 2018;**25**(1):15–31.
39. Zhao M, Wang JT. A stress artificial boundary in FEA for near-field wave problem. *Acta Mechanica Sinica*, 2006;**38**(1):49.

Received: 5 November 2024; **Revised:** 6 February 2025; **Accepted:** 14 March 2025